# A Novel Thermoplastic Elastomer by Reaction-Induced Phase Decomposition from a Miscible Polymer Blend

**Yongjin Li,*,† Yuko Oono,† Yuji Kadowaki,‡ Takashi Inoue,‡ Kazuo Nakayama,† and Hiroshi Shimizu†**

*Nanotechnology Research Institute, National Institute of Advanced Industrial Science and Technology (AIST), Tsukuba Central 5, 1-1-1 Higashi, Tsukuba, Ibaraki 305-8565, Japan, and Department of Polymer Science and Engineering, Yamagata University, Yonezawa 992-8510, Japan*

*Received January 24, 2006; Revised Manuscript Received April 7, 2006*

ABSTRACT: A miscible polymer/polymer system, poly(vinylidene fluoride) (PVDF)/acrylic rubber (ACM), was subjected to dynamic vulcanization to yield an oil- and heat-resistant thermoplastic elastomer (TPE). The morphology of the TPE has been investigated by small-angle X-ray scattering (SAXS), dynamic mechanical analysis (DMA), and transmission electron microscopy (TEM). It was shown that phase decomposition occurs during the dynamic vulcanization process and that the TPE consists of a PVDF-rich matrix and ACM-rich cross-linked particles of submicron diameter in which PVDF crystal lamellae are well developed. The TPE displayed excellent mechanical properties, namely, high tensile strength, large elongation at break, and excellent strain recovery from the highly deformed state. It also showed excellent oil and heat resistance. The formation of PVDF lamellae in ACM-rich particles may be the reason for the excellent oil resistance.

## 1. Introduction

Thermoplastic elastomers (TPEs) generated by dynamic vulcanization have attracted much attention because these materials have the processing characteristics of thermoplastics and the elastomeric characteristics of thermoset rubbers.[1−9] The dynamic vulcanization of an immiscible rubber/plastic system leads to a two-phase material in which cross-linked rubber particles are dispersed in the plastic matrix. Such morphology generation is prerequisite for TPE; i.e., the plastic component should be the matrix to provide the melt processability.

Recently, we have found that poly(vinylidene fluoride) (PVDF) is miscible with acrylic rubber (ACM) in an ACM-rich system and partially miscible in a PVDF-rich system.[10] A static vulcanization of the single-phase mixtures would result in a three-dimensionally cross-linked material which cannot be processed by melt processing methods.[11,12] In contrast, the dynamic vulcanization is expected to induce phase decomposition because (i) at the early stage of vulcanization a microgel (loosely cross-linked domain) is usually formed, (ii) the gel would be hardly coalescence with each other under high shear forces (dynamic state), (iii) the increase in molecular weight and the cross-linking are unfavorable for the polymer−polymer miscibility so that the non-cross-linkable PVDF chains in the microgel particles would be forced to get out, and (iv) the phase decomposition would proceed during the dynamic vulcanization to result in the ACM-rich cross-linked particles and the PVDF-rich non-cross-linked matrix. This morphology may be desirable for TPE. This is why we tried the dynamic vulcanization of a miscible PVDF/ACM system. To the best of our knowledge, this is the first trial on the dynamic vulcanization of a miscible polymer/polymer system.

* To whom correspondence should be addressed. E-mail: yongjin-li@aist.go.jp.

† National Institute of Advanced Industrial Science and Technology (AIST).

‡ Yamagata University.

## 2. Experimental Section

**2.1. Materials and Sample Preparation.** The PVDF and ACM samples used were commercially available KF850 (Kureha Chemicals, Japan) and AR32 (Nippon Zeon Co., Ltd.), respectively. Curative, hexamethylenediamine carbamate (HMDC), was supplied by Rhein Chemie Co., Ltd. All the polymers were dried in a vacuum oven at 80 °C for at least 12 h before processing. The blends without adding curative were prepared using a Brabender-type plastic mixer (Toyoseiki Co., KF70V) with a twin screw at a rotation speed of 100 rpm at 190 °C for 10 min. After blending, all the samples were hot-pressed at 200 °C to a sheet, followed by quenching in ice water. For the preparation of TPE, various amounts of HMDC were added after a 10 min mixing of PVDF and ACM with the same mixer. The mixing was then continued for another 5 min. The melt-mixed sample was then collected and hot-pressed at 200 °C to a sheet, followed by quenching in ice water. The obtained sheets were used for further characterization and property measurements.

**2.2. Structural Characterization.** Dynamic mechanical analysis (DMA) was carried out with a RHEOVIBRON DDV-25FP (Orientec Corp.) in the tensile mode. Dynamic loss (tan $\delta$) was determined at a frequency of 1 Hz and a heating rate of 3 °C/min as a function of temperature from −150 to 120 °C.

Small-angle X-ray scattering (SAXS) patterns were obtained using microfocused Cu K$\alpha$ radiation (45 kV, 60 mA) generated by an X-ray diffractometer (Rigaku Ultrax 4153A 172B) and an imaging plate detector. The exposure time was 6 h for each measurement.

Phase structure was observed by transmission electron microscopy (TEM) (Hitachi H7000) operating at an acceleration voltage of 75 kV. The blended samples were ultra-microtomed at −120 °C to a section with a thickness of about 70 nm. The sections were then stained using ruthenium tetroxide ($RuO_4$) for 20 min.

Differential scanning calorimetry (DSC) was carried out under nitrogen flow at a heating or cooling rate of 10 K/min with a Perkin-Elmer DSC-7 differential scanning calorimeter calibrated with the melting temperatures of indium and zinc. Crystallinity ($\chi_c$) was calculated from the heat of fusion during heating, on the basis of the heat of fusion of 105 J/g for a perfect PVDF crystal.[13]

A polarized optical micrograph (POM) was obtained under crossed polarizers from thin microtomed sections with the thickness about 10 $\mu$m by Olympus BX51.

10.1021/ma060181a CCC: $33.50 
Published on Web 05/10/2006

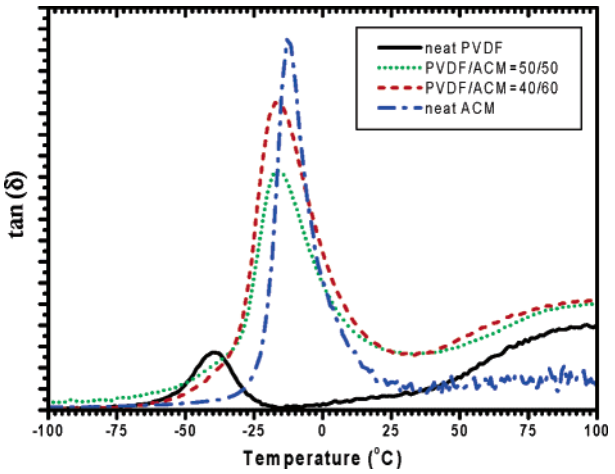


**Figure 1.** Tan $\delta$ vs temperature for neat PVDF, neat ACM, and PVDF/ACM blends.

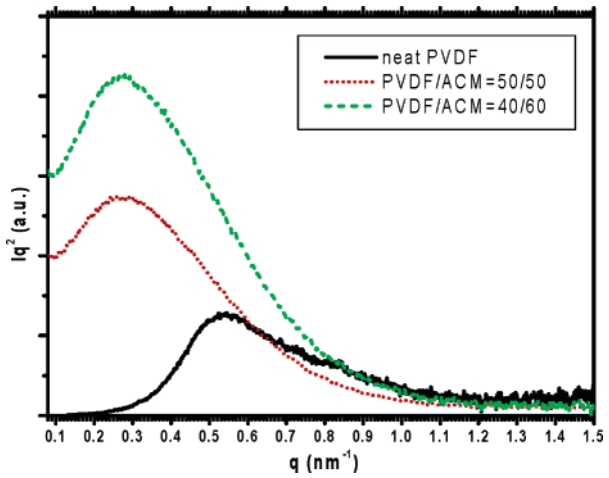


**Figure 2.** Lorentz-corrected SAXS profiles for neat PVDF and PVDF/ACM blends for TPE.

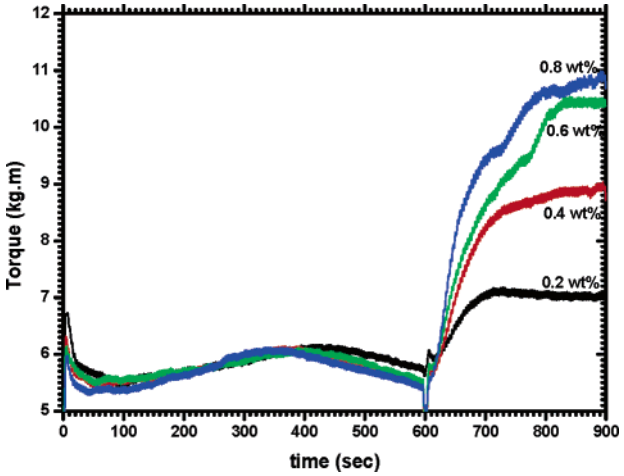


**Figure 3.** Mixing torque vs mixing time for PVDF/ACM 50/50 blend with addition of the indicated curative content.

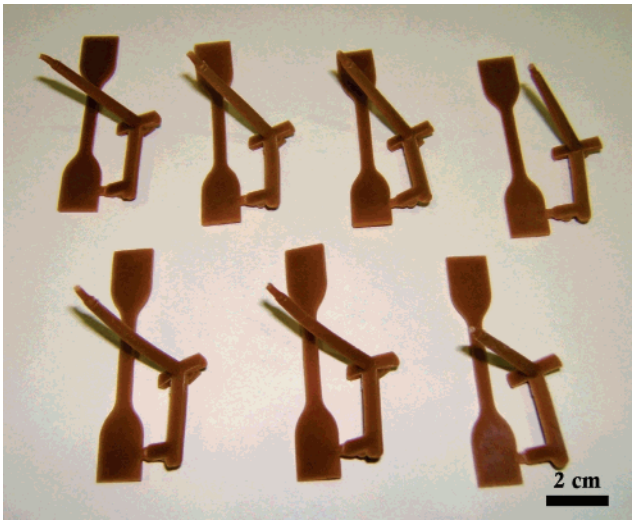


**Figure 4.** Photograph of the injection-molded dumbbell-shaped TPE samples.

**2.3. Physical Property Measurements.** The tensile test was carried out according to the ASTM D 412-80 test method using dumbbell-shaped samples punched out from the molded sheets. The tests were performed using a tensile testing machine, Tensilon UMT-300 (Orientec Co., Ltd.), at a crosshead speed of 500 mm/min at 20 °C and 50% relative humidity. The strain recovery test was also performed as follows: After the preset strain (100% elongation) was attained, the crosshead was returned at the same speed as that when stretching until zero stress was reached.

The heat resistance of TPE was evaluated by measuring the retention of physical properties after a prolonged exposure to hot air. The punched dumbbell-shaped samples were placed in an air oven at 140 °C for 2 weeks. The aged samples were subjected to tensile and strain recovery measurements.

Oil swelling was measured by immersing the samples in toluene at room temperature. Circular samples of 20 mm diameter were punched from the molded sheets with the thickness of about 1−2 mm. After the specified swelling time, the specimens were removed from the solvent and the thickness of the swollen samples was measured. The degree of swelling, $q$, was estimated as

$$q = \frac{l_t - l_o}{l_o} \times 100$$

where $l_o$ is the original thickness of the sample before immersion and $l_t$ is the thickness measured after the specified time of swelling.

## 3. Results

**3.1. Miscibility and Crystal Morphology of PVDF/ACM Blends without Dynamic Vulcanization.** Figure 1 shows plots of the dynamic loss (tan $\delta$) by DMA as a function of temperature for neat PVDF, neat ACM, and PVDF/ACM blends (50/50 and 40/60 w/w ratios). A very broad relaxation peak at about 100 °C and a sharp relaxation peak at −40 °C are observed for the neat PVDF. The former relaxation peak is associated with the molecular motions in crystalline regions, whereas the latter one is assigned to the motion of the main chain in amorphous regions; thus, it is regarded as the glass transition temperature ($T_g$).[14,15] The ACM displays a strong tan $\delta$ peak at −12.8 °C, which corresponds to the $T_g$ of ACM. The blends with 50% and 60% ACM show only one glass transition temperature, which is between the $T_g$s of the PVDF and ACM. These results indicate that the blends are of single-phase nature in amorphous regions. With increasing ACM content, the glass transition temperature increases.

Figure 2 displays the Lorentz-corrected SAXS profiles of the neat PVDF and PVDF/ACM blends used for TPE. The SAXS intensity was normalized by thickness and exposure time after subtracting air scattering from the observed profiles. The neat PVDF exhibits a weak scattering peak at $q = 0.55$ nm$^{-1}$, corresponding to a crystal long period of $L = 11.4$ nm. On the other hand, both blends show a very strong and symmetric scattering peak at about $q = 0.25$ nm$^{-1}$, corresponding to a crystal long period of $L = 25.1$ nm. The scattering intensity

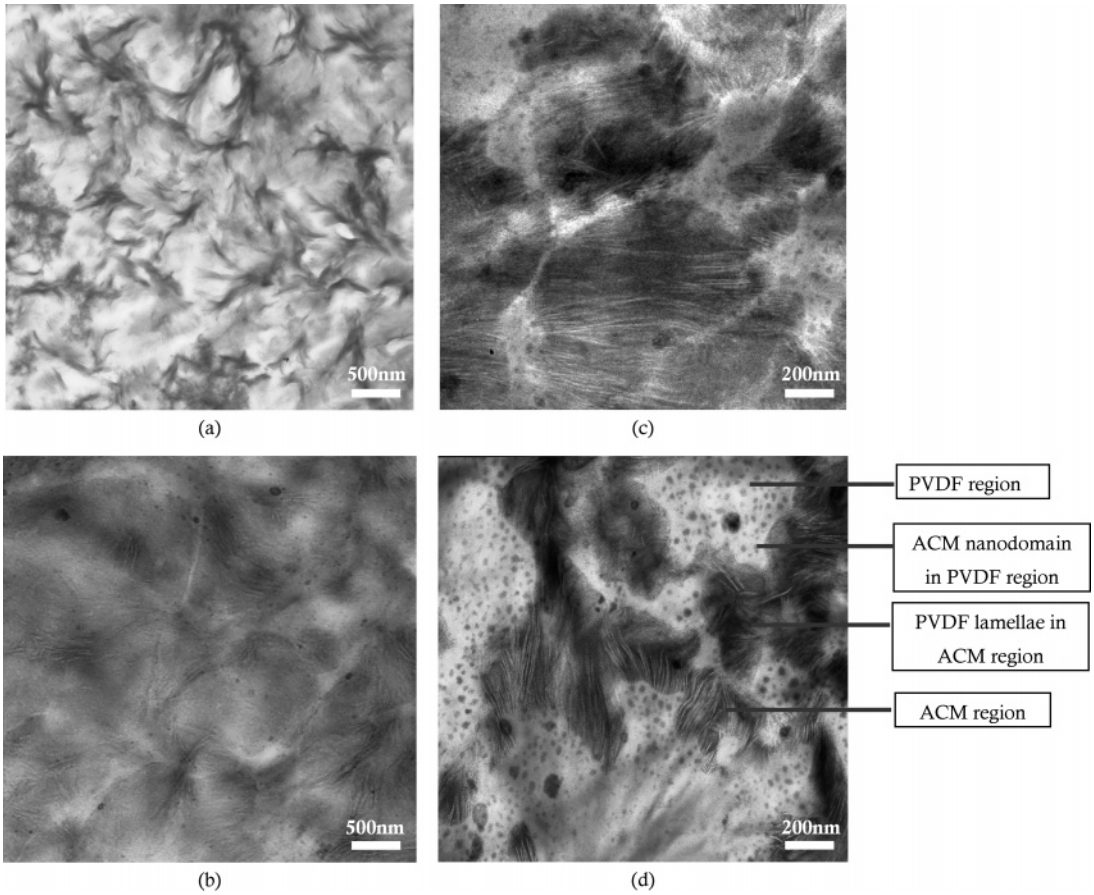


**Figure 5.** TEM images of the PVDF/ACM blends dynamically vulcanized with (a) 0, (b) 0.2, (c) 0.4, and (d) 0.8 wt % curative.

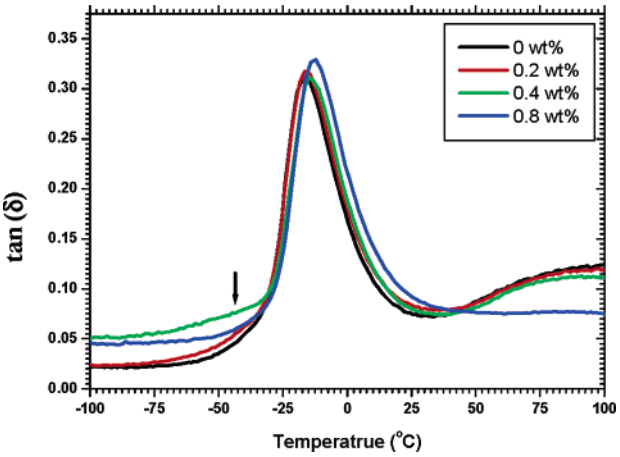


**Figure 6.** Tan $\delta$ vs temperature for PVDF/ACM blends dynamically vulcanized with indicated curative content.

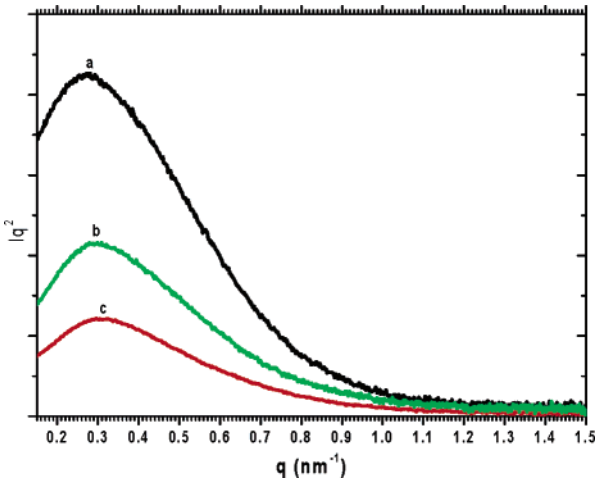


**Figure 7.** Lorentz-corrected SAXS profiles for PVDF/ACM blends: (a) nonvulcanized, (b) dynamically vulcanized with 0.4 wt % curative, and (c) dynamically vulcanized with 0.8 wt % curative.

enhancement can be attributed to the incorporation of ACM molecular chains in the regions between the individual PVDF lamellae. Since the electron density of the ACM is much lower than that of the amorphous PVDF, the insertion of ACM between individual PVDF lamellae would inevitably enhance the electron density contrast between the crystalline and amorphous layers and consequently gives rise to stronger scattering intensity. On the other hand, the crystal long period is also greatly increased from 11.4 to 25.1 nm by the incorporation of ACM chains into the PVDF lamellae. The incorporation of ACM in the amorphous region between PVDF lamellae supports the miscibility between ACM and PVDF.

**3.2. Dynamic Vulcanization and Melt Processability.** Throughout the blending of PVDF and ACM and the dynamic vulcanization of the resulting blend in the batch mixer, the mixing torque was recorded. The mixing torque as a function of mixing time with various curative amounts is presented in Figure 3. Note here that curative was added after a 10 min mixing of PVDF and ACM. A large increase in torque is observed with the addition of curative, indicating the cross-linking of ACM rubber. A higher curative content results in a stronger increase in mixing torque, suggesting a higher cross-link density. As shown in Figure 3, the mixing torque levels off eventually. This indicates that the system is still melt-processable even after the dynamic vulcanization of the miscible blend. Actually, the dynamically vulcanized sample was suc-

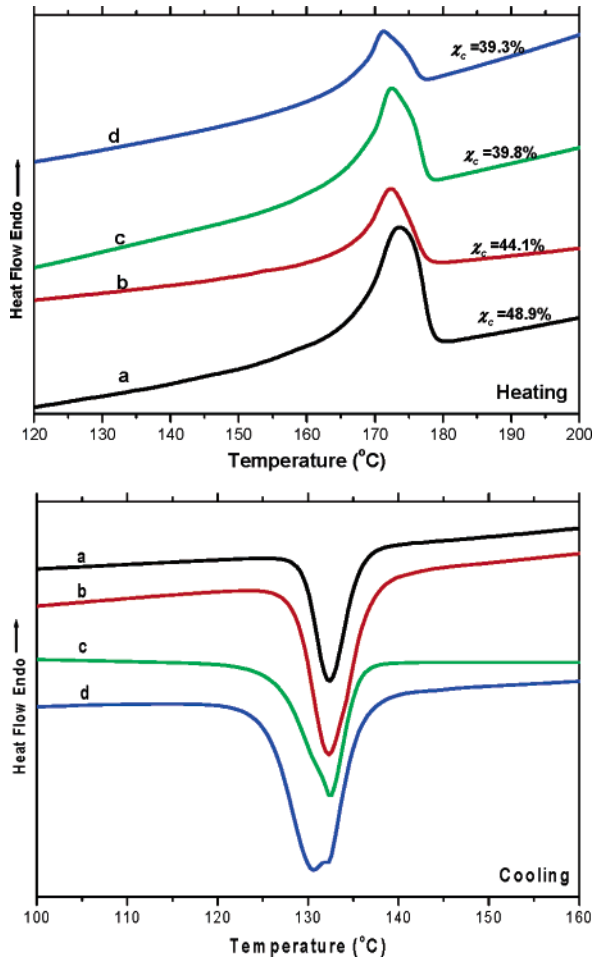


**Figure 8.** DSC heating and cooling diagrams of the PVDF/ACM blends with (a) 0, (b) 0.2, (c) 0.4, and (d) 0.8 wt % curative.

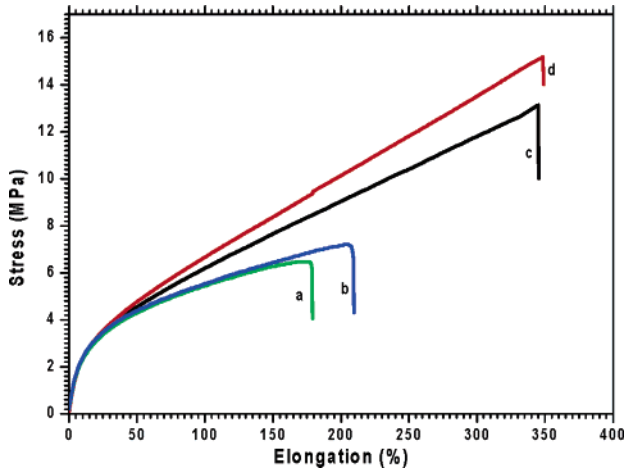


**Figure 9.** Strain−stress curves for the PVDF/ACM TPEs dynamically vulcanized with (a) 0, (b) 0.2, (c) 0.4, and (d) 0.8 wt % curative.

cessfully melt-pressed to a thin sheet. In addition, the dynamically vulcanized TPE can also be processed by normal melt processing methods, such as extrusion and injection molding. Figure 4 shows a photograph of the dumbbell-shaped samples from the TPE produced using injection molding. Moreover, the system was nicely reprocessed for several times: the molded sheet was ground and then melt-pressed to sheet; this was successfully repeated four times.

**3.3. Morphology of Dynamically Vulcanized PVDF/ACM Blends.** The melt-processability of the dynamically vulcanized

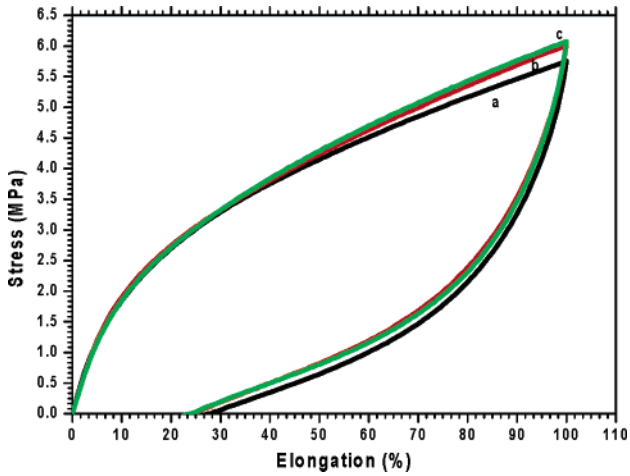


**Figure 10.** Strain recovery curves for PVDF/ACM TPEs dynamically vulcanized with (a) 0, (b) 0.4, and (c) 0.8 wt % curative.

**Table 1. Comparison for Physical Properties of the PVDF/ACM TPE before and after Aging at 140 °C for 2 Weeks**

| | tensile strength (MPa) | modulus (MPa) | elongation at break (%) | residual strain (%) | swell in toluene (%) |
|---|---|---|---|---|---|
| before aging | 14.9 | 25.6 | 351.5 | 27.5 | 23.2 |
| after aging at 140 °C, 2 weeks | 16.2 | 28.9 | 342 | 26.3 | 21.5 |

blends may imply that the matrix should consist of the thermoplastic PVDF or PVDF-rich phase. In other words, the phase decomposition is expected by the cross-linking of ACM from the single-phase blend. The phase structures of the PVDF/ACM initial blend and the dynamically vulcanized TPE as observed by TEM are shown in Figure 5. The initial blend shows a homogeneous phase morphology with small PVDF spherulites dispersed inside, as shown in Figure 5a. This indicates that PVDF and ACM form a one-phase mixture before the dynamic vulcanization, as also displayed by DMA results. However, for the dynamically vulcanized samples, a phase-separated structure can be clearly observed. ACM is observed as the dark phase and PVDF is observed as the bright phase because ACM is more easily stained by $RuO_4$ than PVDF. It is seen that cross-linked ACM particles of submicron diameter are dispersed in the PVDF matrix. In the PVDF matrix, many ACM domains with the size of several tens of nanometers are observed. In ACM particles, PVDF crystal lamellae are seen. The thick lamellae are well developed to several hundred nanometers in length. Note that lamellae are hardly observed in the PVDF matrix because PVDF cannot be stained by $RuO_4$. In addition, it is interesting to note that the phase contrast between PVDF matrix and ACM particles increases with increasing curative content from 0.2 to 0.8 wt % based on both polymers, suggesting a higher degree of phase decomposition as a result of a higher cross-link density caused by loading larger amounts of curative.

**3.4. Miscibility and Crystal Morphology of Dynamically Vulcanized PVDF/ACM Blends.** Figure 6 shows the temperature dependence of tan $\delta$ for the dynamically vulcanized PVDF/ACM blends with various curative contents. Only one relaxation peak at −17.5 °C is observed for the PVDF/ACM blend without curative, indicating a miscible state between the ACM and PVDF amorphous region. The peak shifts to a higher temperature with increasing the curative content. For the TPE with 0.8 wt % curative, the relaxation peak is at −13 °C, which is almost same as the $T_g$ of the neat ACM. On the other hand, a small relaxation shoulder can be discerned at −35 °C for the TPE with a high curative loading content. The shoulder appears

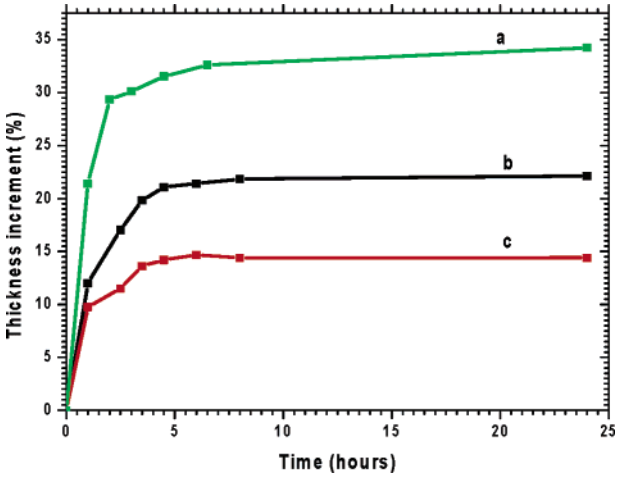


**Figure 11.** Swelling in toluene for the PVDF/ACM TPEs dynamically vulcanized with (a) 0, (b) 0.4, and (c) 0.8 wt % curative.

near the $T_g$ of the neat PVDF. This suggests that the matrix is almost pure PVDF. Referring to the TEM results in Figure 5, it should be noted that the matrix consists of the neat PVDF and the segregated ACM domains. Therefore, the DMA results indicate that the phase decomposition took place by the cross-link reaction. In addition, the broad relaxation peak from PVDF crystalline region at about 100 °C disappears for the sample with 0.8 wt % curatives. This may be attributed to the greatly fragmented PVDF crystals for this highly cross-linked sample (see Figure 13c in the Discussion section).

Figure 7 displays the Lorentz-corrected SAXS profiles of the dynamically vulcanized PVDF/ACM blends with various curative contents. Several characteristic changes with increasing the curative content are observed. First, the scattering intensity decreases progressively with increasing the curative content. This indicates that the electron density difference between the crystalline and amorphous regions decreases, implying that the ACM molecules are expelled out from the PVDF amorphous region between adjacent lamellae by the cross-linking of ACM during the dynamic vulcanization process. Second, the scattering peak of the dynamic vulcanized PVDF/ACM blends shifts from $q = 0.25$ nm$^{-1}$ for the initial blend to $q = 0.31$ nm$^{-1}$ for the TPE with 0.8 wt % curative. It means that the average crystal long period of PVDF decreases from 25.1 to 20 nm by the dynamic vulcanization. The decreasing of the crystal long period again indicates the expulsion of ACM chains from the amorphous region of PVDF. Finally, the shape of the scattering peak becomes broader for the dynamic vulcanized TPE as compared with that without curative, indicating a wider distribution of the long period of PVDF crystals, in other words, less ordered lamellar spacing.

Figure 8 presents DSC curves for the dynamically vulcanized PVDF/ACM blends during heating and cooling at a rate of 10 K/min. PVDF crystallinity ($\chi_c$) for each sample was calculated from the heat of fusion during heating and is shown in Figure 8a. PVDF crystallinity decreases with increasing the cross-link density for TPE, which is consistent with the SAXS results in Figure 7. On the other hand, the samples with 0.4 and 0.8 wt % curative show very broad melting and crystallization peaks compared with the initial blend, indicating more than one type of PVDF crystals located in TPEs.

**3.5. Physical Properties of TPE.** Figure 9 shows the stress−strain curves for TPEs with various curative contents. Both tensile strength and elongation at break increase with increasing curative content. Thus, the tensile properties are improved by increasing the cross-link density of the rubber phase. However, a high cross-link density results in the poor processability of TPEs, as shown in Figure 3 with the increase in mixing torque.

Figure 10 presents the stress−strain recovery behavior of the TPEs with different cross-link densities. The TPEs show excellent elastic recovery. The residual strain is less than 30%, which is smaller than that of the commercialized PP/EPDM TPE with extension oil.[16] A higher cross-link density of the ACM phase provides a slightly higher elasticity.

Table 1 shows a comparison of the physical properties of the TPE with 0.8 wt % curatives before and after aging at 140 °C for 2 weeks in an air oven. One can see that there is almost

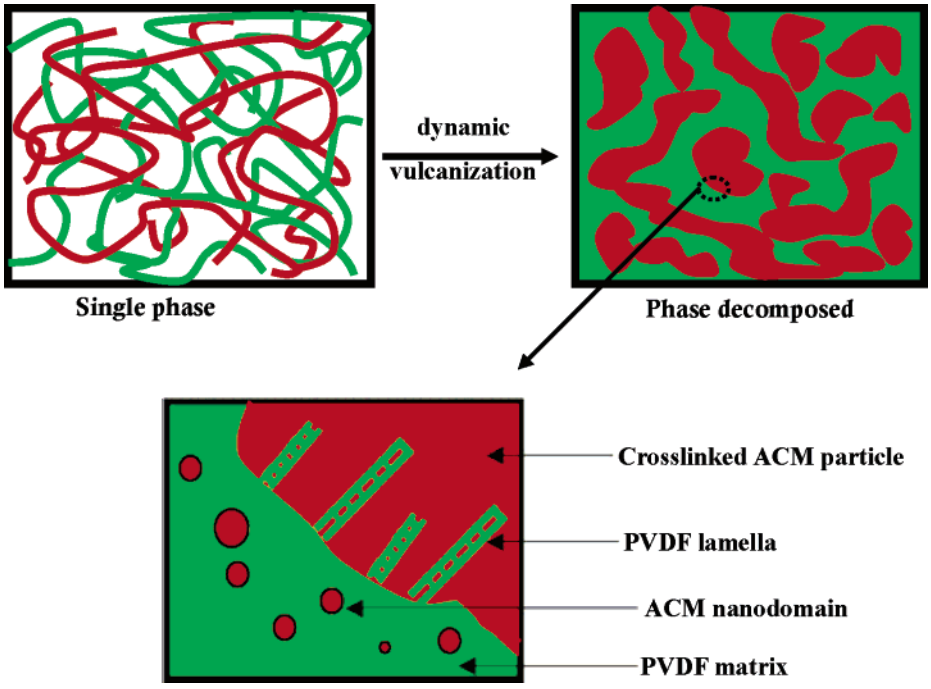


**Figure 12.** Schematic diagram of dynamic vulcanization-induced phase decomposition and the morphology of the TPE (red part indicates the ACM and the green part indicates PVDF).

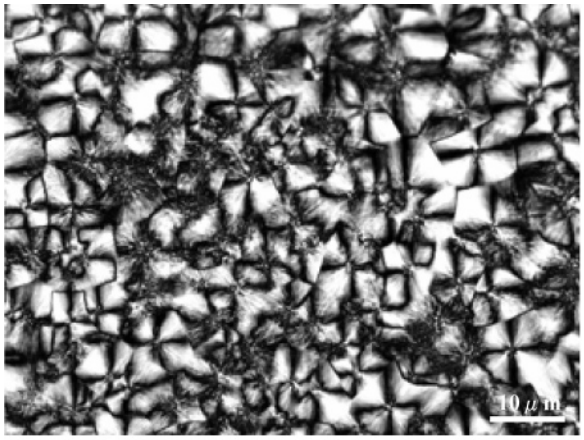


(a)

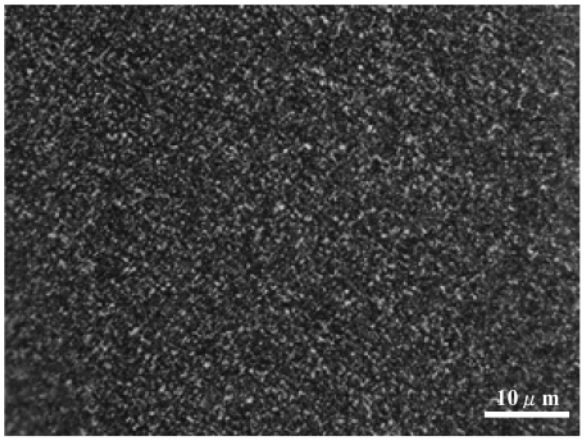


(b)

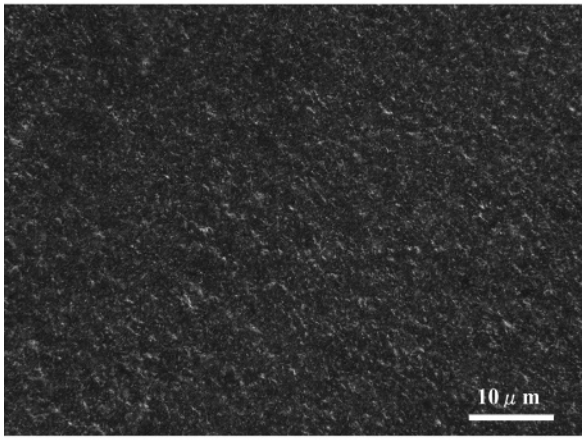


(c)

**Figure 13.** Optical micrographs of (a) neat PVDF, (b) PVDF/ACM (99/1) blend, and (c) PVDF/ACM TPE with 0.8 wt % curative (thin sections were cut through the thickness direction of the hot pressed films).

no change in tensile strength or elongation at break with the aging. The strain recovery is improved by the aging. Thus, an excellent retention of tensile properties after high-temperature aging suggests an excellent heat resistance of the TPE.

Figure 11 shows the swelling behavior of the TPE. The degree of swelling is shown as a function of the time of immersion in toluene at room temperature. The TPE swells in toluene by less than 40% depending cross-link density, which is much lower than the degree of swelling (157−263%) of the commercialized PP/EPDM TPE.[17] By increasing curative content, the degree of swelling decreases markedly.

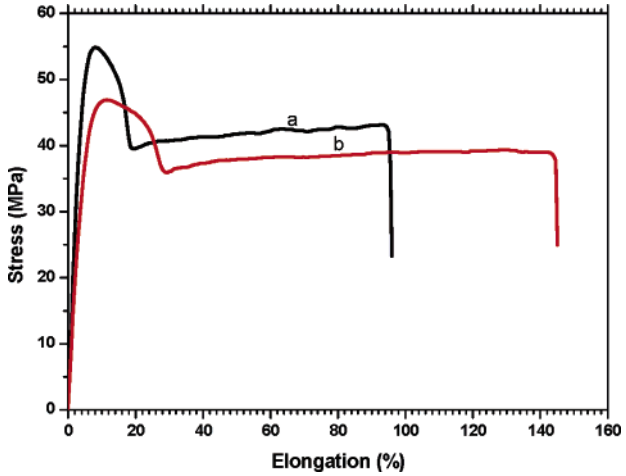


**Figure 14.** Strain−stress curves for (a) neat PVDF and (b) PVDF/ACM 99/1 blend.

## 4. Discussion

A new TPE has been successfully prepared by the dynamic vulcanization of the miscible PVDF/ACM blend. The obtained TPE has a complex morphology in which many ACM nanodomains are dispersed in the PVDF matrix and PVDF crystal lamellae are located in the cross-linked ACM particles. Figure 12 shows a schematic drawing of the cross-link induced phase decomposition process and the morphology of the dynamically vulcanized PVDF/ACM TPE. The miscibility between PVDF and ACM is expected to be caused by the specific interaction between the $CF_2$ dipole of PVDF and the carbonyl group of ACM, as in the case of PVDF blends with many polymers containing carbonyl groups.[18−22] A cross-link reaction imposed on ACM might disturb this specific interaction and lead to phase decomposition. In addition, the cross-linking of ACM causes a significant molecular weight increase for ACM. This leads to a decrease in the entropy of mixing, which is unfavorable for the miscibility.[23−26] These may be the reasons for the phase decomposition by the cross-link reaction. However, partial miscibility seems to still be preserved after the dynamic vulcanization in the melting state. During the subsequent cooling to room temperature, PVDF chains crystallize and segregate out as crystal lamellae in ACM particles, and a small amount of ACM is expelled out during the crystallization of PVDF as the nanodomains in the PVDF matrix, as seen in Figure 5.

The PVDF-rich matrix provides the melt processability of the final TPE. A small amount of ACM in the matrix may play an important role in the excellent strain recovery properties of TPE. It is considered that the ACM may act as impurity to render the smaller and less ordered spherulites of PVDF, which suffer the less plastic deformation of PVDF matrix. That is, the small amount of ACM is expected to make the matrix more elastic, as compared with neat PVDF. It is well-known that the neat PVDF crystallizes into big and ordered spherulites and shows clear yielding and very poor strain recovery after plastic deformation. By contrast, the small amount of ACM in the PVDF matrix causes fragmented crystallites and makes the PVDF spherulites more deformable. Figure 13 shows POM photographs of neat PVDF, PVDF/ACM blend with only 1% ACM, and the TPE with 0.8 phr curative. The mechanical properties of the corresponding neat PVDF and PVDF/ACM 99/1 blend are shown in Figure 14. Large spehrulites are clearly observed in the neat PVDF (Figure 13a), which show a high modulus (1.40 GPa), a clear yielding, and a low elongation at break (95%) during stretching (Figure 14a). In contrast, the

PVDF crystallizes into much smaller and disordered spherulites with the addition of even only 1% ACM, as shown in Figure 13b. The blend displays a lower modulus (0.99 GPa) and a larger elongation at break (145%) than the neat PVDF. On the other hand, the dynamically vulcanized TPE gives even smaller and less ordered spherulites than the PVDF/ACM 99/1 blend, as shown in Figure 13c. Therefore, the PVDF matrix containing ACM is less plastic and more elastic than the neat PVDF; it provides a significant contribution to the mechanism of excellent strain recovery of the TPE.

## 5. Conclusion

We have succeeded in preparing a novel thermoplastic elastomer from a miscible PVDF/ACM blend. Phase decomposition in the miscible PVDF/ACM blend is induced by the cross-linking of ACM during the dynamic vulcanization process. The obtained TPE has a unique morphology: the matrix consists of disordered PVDF spherulites and a small amount of ACM nanodomains, while the dispersed particles are cured ACM with well-developed PVDF crystal lamellae inside. This TPE has excellent physical properties, namely, high elongation at break, nice strain recovery, and excellent heat and oil resistances.

**Acknowledgment.** This work is supported by the New Energy and Industrial Technology Development Organization (NEDO) for the "Project on Nanostructured Polymeric Materials". The authors thank the reviewers for valuable suggestions.

## References and Notes

(1) Coran, A. Y.; Patel, R. P. *Rubber Chem. Technol.* **1980**, *53*, 141.
(2) Coran, A. Y.; Patel, R. P.; Williams, D. *Rubber Chem. Technol.* **1982**, *54*, 1063.
(3) Coran, A. Y.; Patel, R. P. *Rubber Chem. Technol.* **1983**, *56*, 1045.
(4) Coran, A. Y.; Patel, R. P.; Williams, D. *Rubber Chem. Technol.* **1985**, *58*, 1014.
(5) George, J.; Ramamurthy, K.; Varughese, K. T.; Thomas, S. *J. Polym. Sci., Polym. Phys.* **2000**, *38*, 1104.
(6) Oderkerk, J.; Groeninckx, G.; Soliman, M. *Macromolecules* **2002**, *35*, 3946.
(7) Ma, P. L.; Favis, B. D.; Champagne, M. F.; Huneault, M. A.; Tofan, F. *Polym. Eng. Sci.* **2002**, *42*, 1976.
(8) Ellul, M. D.; Tsou, A. H.; Hu, W. G. *Polymer* **2004**, *45*, 3351.
(9) Sirisinha, C.; Saeoui, P.; Guaysomboon, J. *Polymer* **2004**, *45*, 4909.
(10) Li, Y. J.; Oono, Y.; Nakayam, K.; Shimizu, H.; Inoue, T. *Polymer* **2006**, *47*, in press.
(11) Wallace, J. G. *Handbook of Thermoplastic Elastomers*, 2nd ed.; Springer: New York, 1988; Chapter 5.
(12) Paul, D. R.; Bucknall, C. B. *Polymer Blends*; Wiley-Interscience: New York, 2000; Vol. 2, Chapter 35.
(13) Nakagawa, K.; Ishida, Y. *J. Polym. Sci., Polym. Phys.* **1973**, *11*, 2153.
(14) Kakutani, H. *J. Polym. Sci., Part A-2* **1970**, *8*, 1177.
(15) Yano, S.; Tadano, K.; Aoki, K.; Koizumi, N. *J. Polym. Sci., Polym. Phys. Ed.* **1974**, *12*, 1875.
(16) Yang, Y.; Chiba, T.; Saito, H.; Inoue, T. *Polymer* **1998**, *39*, 3365.
(17) Bailey, M. A.; Costin, C. R.; Lohr, J. E. www.sartomer.com/wpapers/5523.pdf.
(18) Penning, J. P.; Manley, R. St. J. *Macromolecules* **1996**, *29*, 77.
(19) Rahman, M. H.; Nandi, A. K. *Macromol. Chem. Phys.* **2002**, *203*, 653.
(20) Bernstein, R. E.; Paul, D. R.; Barlow, J. W. *Polym. Eng. Sci.* **1978**, *18*, 1225.
(21) Becke, R. E.; Cabasso, I. *Polymer* **1988**, *29*, 1831.
(22) Nishi, T.; Wang, T. T. *Macromolecules* **1975**, *8*, 909.
(23) Vanden Poel. G.; Goossens, S.; Goderis, B.; Groeninckx, G. *Polymer* **2005**, *46*, 10758.
(24) Lee, J.; Yandek, G. R.; Kyu, T. *Polymer* **2005**, *46*, 12511.
(25) Ramanujam, A.; Kim, K. J.; Kyu, T. *Polymer* **2000**, *41*, 5375.
(26) Schmidt, R. H.; Haupt, K. *Chem. Mater.* **2005**, *17*, 1007.

MA060181A